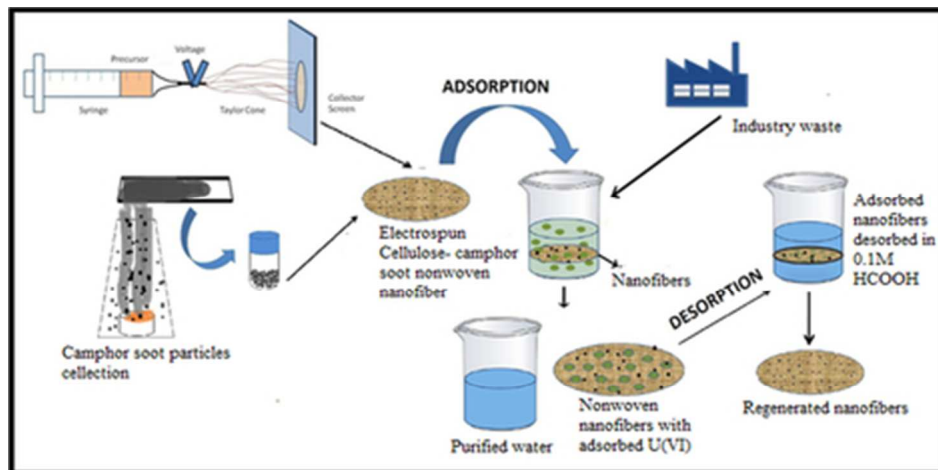




An effective Technique for Removal and Recovery of Uranium (VI) from Aqueous Solution Using Cellulose-Camphor Soot Nanofibers

Journal:	<i>RSC Advances</i>
Manuscript ID:	RA-ART-02-2014-001751.R1
Article Type:	Paper
Date Submitted by the Author:	12-May-2014
Complete List of Authors:	Singh, Nitesh; Vellore Institute of Technology, Chemistry KANDASUBRAMANIAN, BALASUBRAMANIAN; DIAT(DU), METATERIALS ENGINEERING



39x19mm (300 x 300 DPI)

Cite this: DOI: 10.1039/c0xx00000x

www.rsc.org/xxxxxx

An effective Technique for Removal and Recovery of Uranium (VI) from Aqueous Solution Using Cellulose- Camphor Soot Nanofibers

Nitesh^a, Balasubramanian K^{b*}*Received (in XXX, XXX) Xth XXXXXXXXXX 20XX, Accepted Xth XXXXXXXXXX 20XX*

DOI: 10.1039/b000000x

Speciation and recover of U(VI) ions from nuclear wastewater is a heavy challenge for various nuclear centers and research organizations. In this perspective, the present research work aims at using cost effective cellulose nanofibers for reclamation of these incurable ions. Cellulose nanofibers were synthesized by electrospinning technique and functionalized with carbon nanoparticles (CNPs) obtained from the camphor soot, having noticeable metal sorption capacity. Sorption capability was ascertained by conducting systematic batch experiments for optimization of parameters like CNP dosage, pH selectivity, and dosage of nanofibers. The results indicated fast uptake of U(VI) ions, significantly observed at pH 6 with the adsorption percentage of 97 from mimicked solution within a period of 120 minutes. 85% of U(VI) was removed from aqueous solution with an adsorbent dosage of 50mg. The maximum adsorption capacity was noted to be 410mg/g with 96% adsorption at varying concentration within a period of 60min. Adsorptive uptake capacity of U(VI) ions was described with Adsorption isotherms (Langmuir, Freundlich, Temkin and Dubinin-Radushkevich). Pseudo first order and Elovich model defined the sorption kinetics with good correlation regression values ($R^2= 0.99$). The cellulose- camphor soot nanofibers were characterized through field emission scanning electron microscopy (FESEM), Fourier transform infrared-spectroscopy (FT-IR), X-ray diffraction (XRD) and Raman spectroscopy. Further, thermodynamic parameters such as standard free energy (ΔG_0), standard enthalpy (ΔH_0) and standard entropy (ΔS_0) reveals that adsorption process was an endothermic and spontaneous process for uptake of U(VI) ions. Reusability of the fibers was effectively done with 0.1M CH_3COOH and HCOOH with a contact time of 30 min.

1. Introduction

Extensive application of U(VI) has resulted in production of various gaseous, liquid and solid wastes containing uranium isotopes which are released in the surface or underground water streams¹. U(VI) has gained immense popularity in nuclear fuel industry, catalysis, optics, aeronautics, aerospace, high temperature ceramics and high quality lenses² over the past few years.

^aDepartment of Chemistry, Vellore Institute of Technology (VIT), Vellore- 632014, India, Email: singh.nitish24@gmail.com

^{b*}Department of Materials Engineering, DIAT (DU), Girinagar, Pune, Maharashtra, Ministry of Defence, Email: meetkbs@gmail.com, Fax: (020) 2438-9509, Tel (020) 2438-9680);

U(VI) requires a slightly different approach for the evaluation of adverse health effects because they release electromagnetic radiations which causes lethal diseases such as lung, pancreatic and liver cancer³. U(VI) gets immediately removed from the solution to particles with an average residence period of <100 years and gets deposited at the bottom of the sea which has resulted in 10 pg/ml of U(VI) concentration in sea water⁴. Various techniques employed for the removal and recovery of radioisotopes from wastewaters include chemical precipitation, ion exchange, membrane-related processes, biological processes and electrochemical techniques, which however, possess major disadvantage of being time-consuming processes, high costs, generation of toxic wastes⁵. Amongst these, natural polymeric materials as adsorbent have attracted immense interest for remediation of heavy and toxic metal ions due to their biodegradability, flexibility, lower consumption of reagent and non-toxic nature⁶.

Cellulose is the most abundant bio-renewable biopolymer with an extensive network of intra and inter-hydrogen bonds which enables it to adopt a highly ordered structure. Such ordered structure is responsible for desirable chemical and mechanical

properties which also accounts for cellulose being insoluble in most of the solvents⁷⁻⁸. Research has been focused on synthesis of varied cellulose derivatives possessing enhanced sorption properties towards transition metals and heavy metal ions, which could be used as chelating resins in metal cation separation and extraction of water⁹⁻¹¹.

Carbon Soot particles are the result of incomplete combustion of carbonaceous materials. These particles are primarily composed of carbon and consists of agglomerated particles (particle diameter ~ 10-30 nm)¹²⁻¹³. They possess neither graphite nor diamond like structures. The graphite-like crystalline domain is composed of 3-4 turbostratically stacked graphene layers, with an average lateral size of ~ 3 nm and interlayer distances of about 3.5 Å and are known as highly disordered graphitic lattice. Soot particles when released in the atmosphere are known to adsorb pollutants from the air due to their small particle size¹⁴, large specific surface area¹⁵ and long atmospheric lifetime (from several days to weeks)¹⁶. The adsorbed pollutants include heavy metals like Pb, Hg and Cd¹⁶, heavy metal compounds, like MNO_3 and MSO_4 , and organic pollutants like polycyclic aromatic hydrocarbons (PAHs) and volatile organic compounds. Camphoric carbon soot obtained by burning camphor ($\text{C}_{10}\text{H}_{16}\text{O}$) possesses abundant hydrogen in its structure with presence of sp^2 and sp^3 hybridized bonds in camphor molecule¹⁷⁻¹⁸. Out of the ten carbon atoms in camphor, seven are associated in the hexagonal ring system which has an open book type structure (Fig. 1a). The ring structure when observed vertically downward reveals two pentagonal rings (1-2-3-4-7 and 1-4-5-6-7) one on each side of the viewer's vertical plane (Fig. 1b). Camphoric soot can easily provide both hexagonal and pentagonal rings, thus adjusting the deposition conditions of camphoric soot, the sp^3 and sp^2 ratio can be altered¹⁹⁻²⁰.

In this present study, a simple and cost effective route has been adopted in our laboratory for the generation of new kind of nonwoven nanofibers of cellulose acetate functionalized with camphor soot using electrospinning technique which is off low cost, easily available, with high regeneration capacity, used to investigate the adsorption of incurable metal ions from aqueous streams. As a continuation, we have further decided to discuss the morphology of adsorbent and explore the adsorption efficiency for the uptake of U(VI) ions from aqueous streams in batch process under the influence of various experimental parameters like pH selectivity, CNP dosage and dosage of nanofibers to determine the optimum conditions for the maximum removal of heavy metal ions. A separation scheme has been designed based on the sorption isotherms and kinetics data for the removal and necessitous recovery of U(VI) ions from the adsorbent. Also, we characterize the adsorption mechanism of nanofibers through FESEM, FT-IR, XRD and Raman spectroscopic techniques

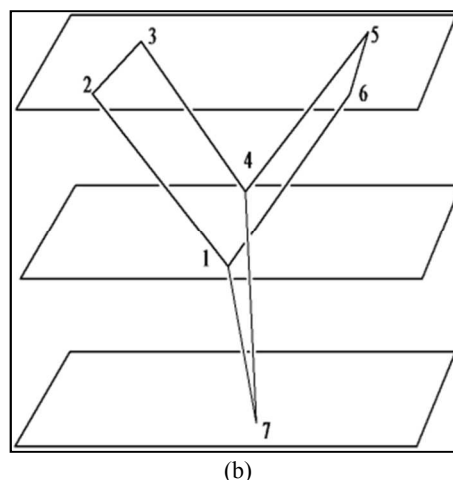
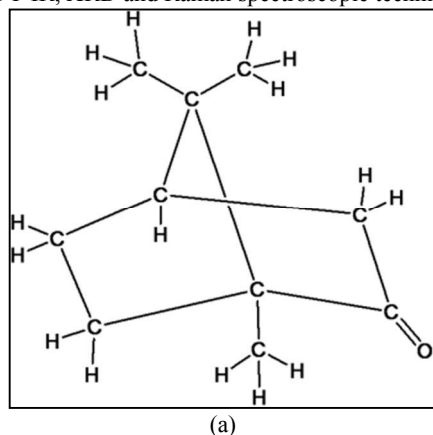


Fig. 1- (a) Open structure of camphor soot (b) Ring structure of camphor soot

2. Experimental

2.1 Materials

Cellulose acetate ($M_w = 30,000$, % acetyl content = 37), Uranium acetate [$(\text{UO}_2(\text{CH}_3\text{COO})_2 \cdot 2\text{H}_2\text{O})$], (2:1) N,N-dimethylacetamide (DMAc) : Acetone, base (NaOH, NH_4OH), acid (HCl, CH_3COOH , HCOOH , $\text{C}_6\text{H}_8\text{O}_7$) and Arsenazo (III) were obtained from Sigma Aldrich, India and used as received. Camphor ($\text{C}_{10}\text{H}_{16}\text{O}$) tablet of size (7×5mm) was used as a precursor for obtaining camphor soot particles without any further purification. De-ionized water was used for all the experiments which were obtained from Millipore Milli-Q system.

2.2 Synthesis of camphor soot particles

A single camphor tablet (7×5mm) was placed in a silica crucible and the entire assembly was kept inside a perforated polycarbonate chamber. The camphor soot particles were collected on a glass substrate in a controlled fashion placed above the flame for 5-10sec. The emitted soot particles are collected in a layered pattern over a glass substrate. The camphor soot particles was carefully removed from the glass sheet without using any metal scraper and stored in a glass bottles for further use without any post treatment¹⁷.

2.3 Electro-spinning of cellulose- camphor soot nanofibers

The electro-spinning setup consists of cellulose acetate solution, an aluminium foil, a grounded electrode, a syringe and needle (internal diameter is 0.42mm) which was connected to a high voltage power supply. The polymer solution was prepared by stirring cellulose acetate, 4% (w/v) in acetone: N,N-dimethylacetamide solvent mixture, $(\text{Me})_2\text{CO}$: DMAc (1:2). The soot particles were sonicated in DMAc for 60 min at 25°C. This mixture was slowly added to the cellulose acetate solution under constant stirring to obtain a homogeneous, viscous and spinnable solution. Three different solutions were prepared with varying carbon content from 0.1 to 0.3wt%. The aluminium foil collector was placed 5cm from the tip of the stainless steel needle and a syringe pump was used to pump the solution at a controlled flow rate of 6 $\mu\text{L}/\text{min}$. The needle was connected to a voltage of 10kV for this work and the spun fibers got collected on the aluminium

foil. After formation of nano fibers, the aluminium foil peeled off and the fibers collected carefully and dried under vacuum to yield white nonwoven nano fibers with varying carbon content (0.1-0.3 wt%).

2.4 Preparation of U(VI) stock solution

U(VI) stock solution with concentration of 1000 mg/L was prepared by dissolving 0.5g Uranium acetate in 1000ml de-ionized water. The desired concentrations (50 – 250 mg/L) were obtained by diluting the stock in de-ionized water.

2.5 Characterization:

FESEM were used to examine the morphology and particle size of the cellulose-camphor soot nanofibers (JSM- 6700F). Functional group analysis was carried out using Fourier Transform infrared (FT-IR) spectrophotometer (Nicolet™-380) in the wavelength range 400-4000 cm^{-1} . Raman spectra's were recorded using the Renishaw in micro- Raman spectrometer using argon laser excitation wavelength of 632.81nm at 20mW power with illumination spot size of 1 μm and acquisition time 90sec. Different samples of cellulose nanofibres were analysed by X-ray diffraction (XRD) using Bruker AXS D8 advance diffractometer with Cu K α radiation.

2.6 Batch sorption studies

Batch sorption studies were conducted to study the removal of heavy metal ions by the adsorbent and attain the equilibration data. The 50mL of Uranium acetate solution of desired concentration (50-250mg/L) was added to 100mL standard flasks. Adsorbate concentration (10mg-50mg) was also varied for different experimental set to obtain different set of data. Dilute CH_3COOH and NH_3 was used for the adjustment of pH (4-8). The flasks were agitated on an orbital shaker at 150 rpm for 15min. Supernatant solution was removed (2.0mL) periodically to analyze the residual U(VI) ion concentration at 0, 60 and 120min.

2.7 Equilibrium Isotherms:

Adsorption isotherm experiments were conducted using optimized experimental parameters (pH-6, camphor content-0.1wt%, adsorbent dosage- 50mg) with varying initial concentrations (50-250mg/L) under ambient temperature 303K. Absorbance was taken at regular time intervals of 10min and the equilibrium adsorption time was assumed to be 120 minutes. The isotherms are plotted in between equilibrium adsorption capacity (q_e) vs. equilibrium concentration of the residual U(VI) ions in the solution. The residual U(VI) ion concentration was calculated spectrophotometrically by complexing with Arsenazo(III) at 655 nm. Adsorption capacity (%Ad) was calculated by the following formula:

$$\% \text{ Adsorption} = \frac{C_0 - C_e}{C_0} * 100 \quad (1)$$

Where, C_0 and C_e are initial metal ion concentration and metal ion concentration at equilibrium²².

2.8 Kinetic Studies:

Kinetic experiments was followed by varying the initial U(VI) ion concentrations (50-250mg/L) in optimized conditions (pH-6, camphor content- 0.1wt%, adsorbent dosage- 50mg, and contact time- 120min). The amount of metal ion adsorbed (q_e) was calculated using the following expression:

$$q_e = \frac{(C_0 - C_e)}{M} * V \quad (2)$$

Where, C_0 and C_e are initial metal ion concentration and metal ion concentration at equilibrium respectively; V = Volume (l); M

= cellulose fibers weight (g); q_e = adsorption capacity at equilibrium time t (mg/g)²².

2.9 Desorption studies

Reusability of adsorbent was done by conducting desorption experiments to analyze U(VI) ion concentration using an aqueous solution of acid (HCl , CH_3COOH , HCOOH , $\text{C}_6\text{H}_8\text{O}_7$) and base (NaOH , NH_4OH). The desorption (%) was calculated from the amount of U(VI) desorbed to the desorption medium and the amount of U(VI) adsorbed on the adsorbent.

3. RESULTS AND DISCUSSION

3.1 Characterization of cellulose- camphor soot nanofibers:

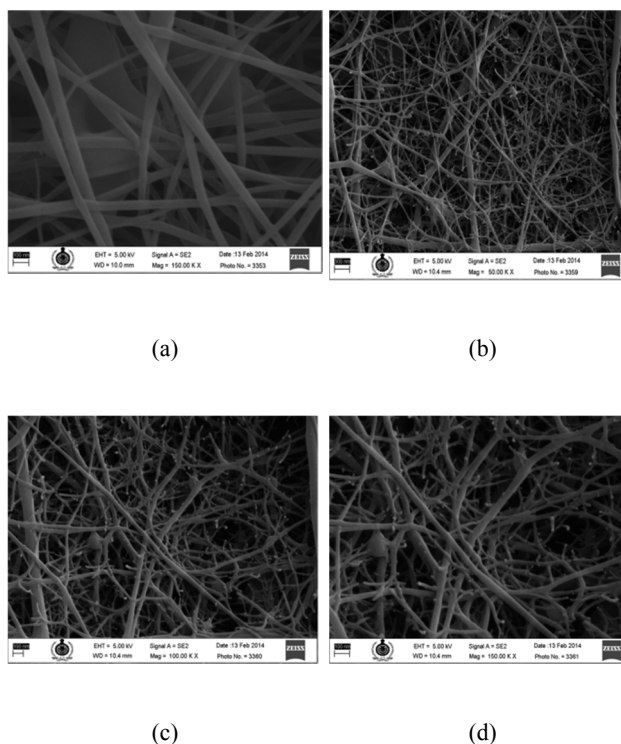


Fig. 2- FESEM Images (a) cellulose electrospun fibers (b) cellulose fibers loaded with camphor soot (c and d) magnified view of CCSF

The FESEM analysis reveals the surface morphology of electrospun fibers of cellulose and cellulose loaded with 0.1 wt% camphor soot particles obtained from combustion of camphor. The unfilled virgin electro spun fibers of cellulose (Fig.2a) were found to have uniform diameter an aspect ratio devoid of porous network. Incorporation of porous camphor soot was found to increase the porosity of the fibers which may increase the adsorption capacity was further confirmed by the BET analysis. The surface area was obtained as 12.1 m^2/g for cellulose acetate fibers which enhanced to 16.96 m^2/g with incorporation of camphor soot reveals interconnected fragile network bonded by weak Vander Waals forces of attraction²¹. These fibers form a chain of carbon nano spheres with an average particle size of 25-50 nm (Fig. 2b) which were seen to be captured in the glassy state of the semi crystalline polymer. Similar morphology also reflects some variation in fiber diameter and also in homogeneity as can be seen in (Fig. 2c), which attributed to the chain of interlinked

carbon nano spheres²². The low magnification image of nano fibers however reflects the compact packing of carbon chain in the cellulose acetate matrix to give a 3-D structure (Fig. 2d).

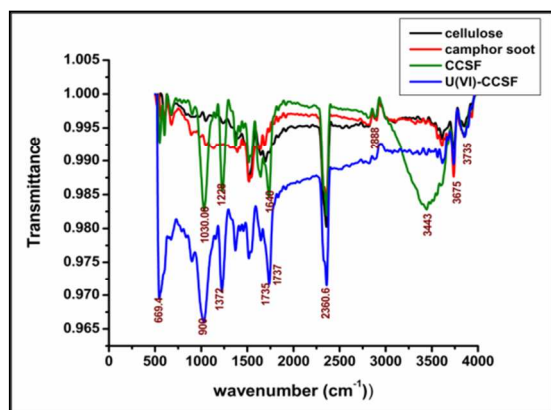


Fig. 3- IR Spectra of cellulose fibers, camphor soot particles, cellulose-camphor soot fibers (CCSF) and U(VI)-CCSF.

The FT- IR spectra of electrospun cellulose fibers, camphor- soot particles, cellulose- camphor soot fibers (CCSF) and U(VI) – cellulose-camphor soot fibers (Fig. 3) shows absorption band at 3443, 2888 and 1640 cm^{-1} because of hydrogen bonded –OH stretching vibration, C-H stretching from the –CH₂ group and –OH bending vibration²³⁻²⁴. The alcoholic free –OH stretching is observed at 3675 and 3735 cm^{-1} . A broad peak is observed at 3443 cm^{-1} which corresponds to the strong interaction of –OH stretching vibration from the acetate group in cellulose acetate and alcoholic group in camphor soot particles. Appearance of sharp peaks at 1735 and 1737 cm^{-1} in CCSF and U(VI)-CCSF confirming the presence of C=O stretching from acetyl group represents the functionalization of cellulose acetate with camphor soot particles. The 1950 to 1450 cm^{-1} region exhibits IR absorption from a variety of double bonded functional groups¹⁷. The peaks at 1280 to 1000 cm^{-1} corresponds to C=O stretching and C-OH in plane bending frequencies of groups such as phenols and carboxylic acid²⁵. The shift of C-O peak to higher frequencies (1223- 1371 cm^{-1}) could be due to high electron density induced by adsorption of U(VI) to the adjacent carbonyl groups²⁶. This shifting represents the coordination between uranyl ion and oxygen atom of the carboxyl group. Thus, presence of characteristic peak at 900 cm^{-1} in U(VI)-CCSF attributed to the asymmetric stretching vibration of UO_2^{2+} indicates higher U(VI) adsorption onto cellulose- camphor soot nanofibers.

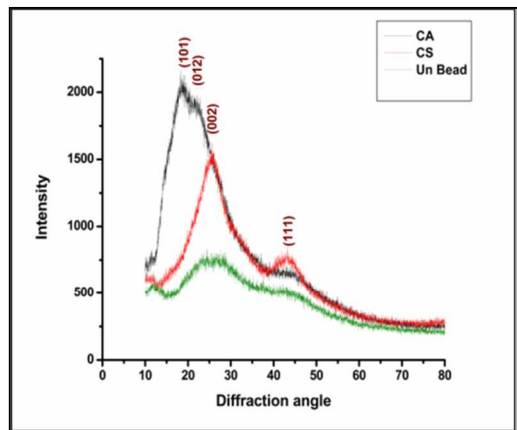
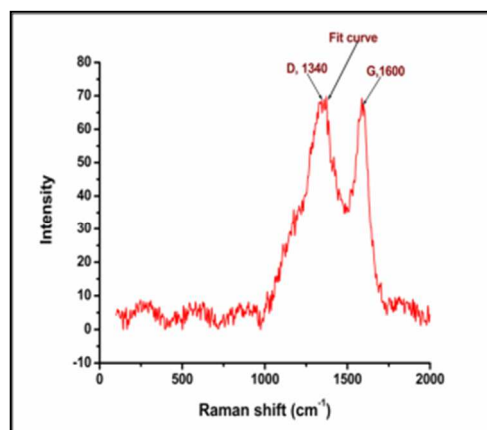
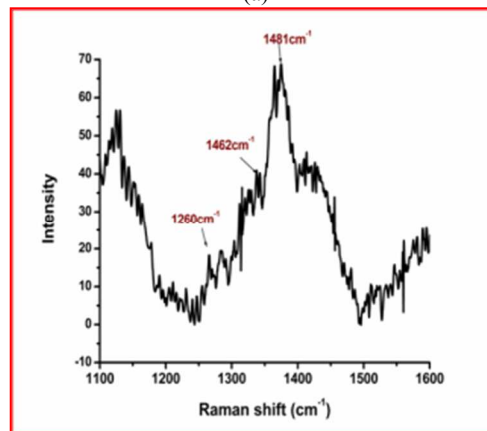


Fig. 4- XRD Patterns of cellulose, camphor- soot particles, cellulose-camphor soot fibers

XRD analysis of cellulose, camphor- soot, CCSF, U(VI)-CCSF are shown in Fig.4. In XRD pattern of cellulose, diffraction peaks appears at $2\theta = 15.9^\circ$ and 22.2° corresponds to partial crystalline nature of cellulose fibers. The peak in camphor- soot particles at 24.65° reveals the presence of large amount of amorphous carbon material. This 2θ value represents to (002) lattice plane. The 2θ value of 42.6° corresponds to (111) lattice which reveals the presence of Diamond like carbon particles. Sahoo *et.al* also made the similar observations²⁷. A broad peak at $20^\circ - 30^\circ$ in CCSF represents the dispersion and exfoliation of cellulose nanofibers to form an integrity type matrix with camphor soot. This diffraction pattern shows an increase in amorphous nature, which may increase the adsorption capacity.



(a)

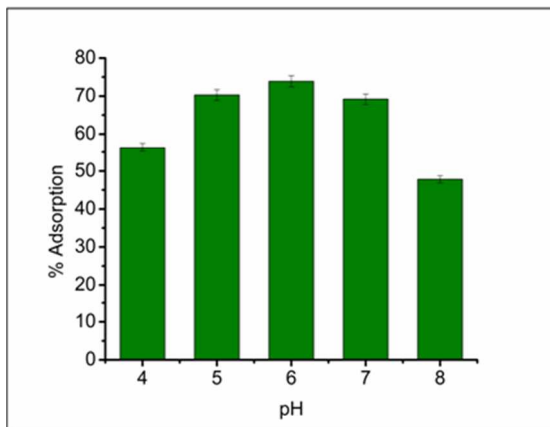


(b)

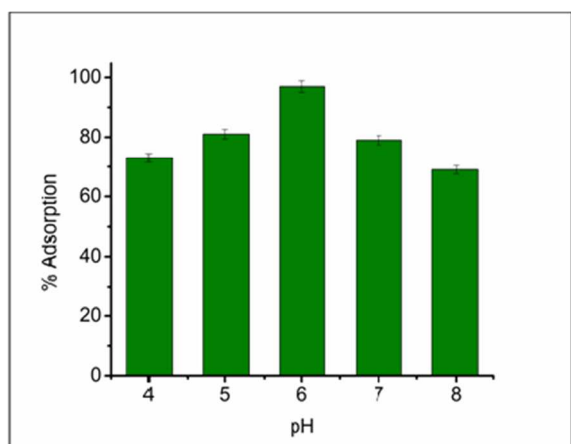
Fig. 5- Raman spectra of (a) camphor soot particles and (b) cellulose acetate fibers

The Raman spectra of camphor soot particles (Fig.5) have shown two distinct bands at 1340cm^{-1} (D band) and 1600cm^{-1} (G band). High intensity of G band at 1600cm^{-1} corresponds to scattering on sp^2 bounded carbon atoms combined with crystalline graphitized carbon and this band also represents to highly oriented pyrolytic carbon. D band observes at 1340cm^{-1} corresponds to scattering on sp^3 bounded amorphous carbon atoms on highly disordered graphene sheets²⁸. A peak is observed at 1462cm^{-1} and 1481cm^{-1} in cellulose fibers represents the vibrational modes of methylene (–CH₂–) bridges and characterize the amorphous and crystalline nature of cellulose. Spectral region of $1510-1210\text{cm}^{-1}$ is preferred to study to increase the adsorption capacity of cellulose fibers with addition of camphor soot particles.

3.2 Effect of pH on Adsorption



(a)



(b)

Fig. 6- Effect of pH on adsorption (a) cellulose acetate fibers (b) cellulose-camphor soot fibers

The pH plays an important role on the protonation and deprotonation of the adsorbent and adsorbate functional groups and enhanced the metal speciation and surface metal binding sites. Camphor soot particles shows no adsorption of U(VI) ion from mimicked solutions at varying pH 4-8 due to its super hydrophobic nature¹⁷ and lack of interaction between uranyl ion and oxygen of the carbonyl group whereas cellulose acetate fibers shows maximum adsorption (Fig. 6a) of 73% at pH 6 because of coordination between metal ion and oxygen of the acetate group. But Adsorption was found to raise significantly from 73% to 97% when pH increases from 4 to 6 under optimized conditions (adsorbent dosage- 50mg, U(VI) concentration-50mg/L, contact time-120min) when cellulose fibers loaded with 0.1wt% camphor soot particles (Fig.6b). After that slight decrease of adsorption efficiency was noted in pH range of 7 to 8. The minimum adsorption was noted at lower pH 4 when the surface of the adsorbent was surrounded by hydronium ions (H^+), thereby removing the metal ions from approaching the binding sites of the

adsorbent²⁹. This means that at higher H^+ concentration, the adsorbent surface becomes more positively charged which reduces the attraction between fibers and the metal cations³⁰.

Further, increase in pH, increases the adsorption capacity resulted in precipitation of U(VI) ion in the form of oxides and availability of more negatively charged surface facilitates the greater U(VI) removal. Therefore, it is concluded that increase in pH increases the adsorption of metal ions due to low stability of metal ionic species in the solution.

3.3 Effect of camphor soot loading on Adsorption

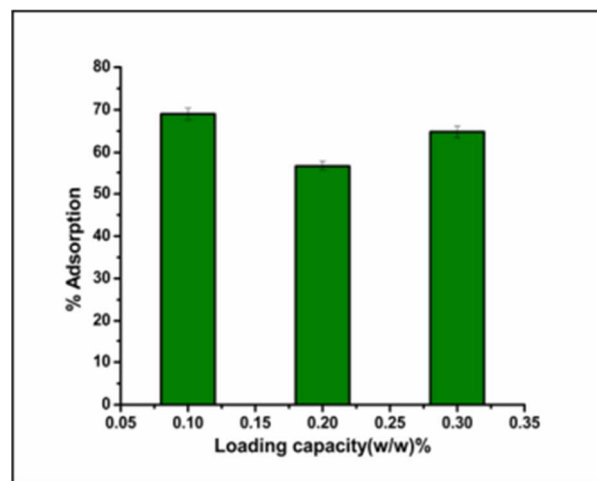


Fig. 7 - Camphor soot loading

Camphor soot content was varied from 0.1- 0.3 wt% in the fiber composition to study the adsorption behavior under optimized conditions (pH-6, adsorbent dosage- 50mg, U(VI) concentration-50mg/L, contact time- 120min). Increase in soot content from 0.1 to 0.3 wt% enhances the adsorption due to increase in active sites ($-C=O$ groups) in the sorbent matrix (Fig. 7). However, further enhance in soot content tends to diminish the efficiency due to compact packing of the fiber which in turn results in steric hindrance to the adsorbing U(VI) ion.

3.4 Effect of sorbent dose on Adsorption

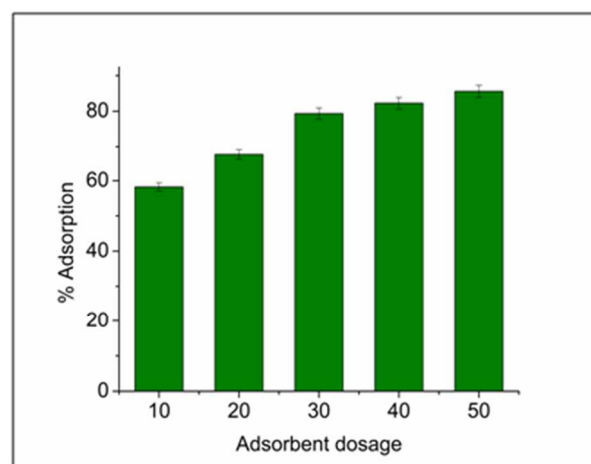


Fig. 8 - Adsorbent dosage

The adsorption efficiency increases from 58% to 85% for U(VI) with increasing amount of adsorbent from 10 mg to 50 mg (Fig. 8) under optimized conditions (pH-6, camphor content-0.1wt%, U(VI) concentration-50mg/L, contact time-120min). Further increase in dosage amount, there is no significant increment observed in adsorption. Therefore, 50mg dosage amount was used in all the studies. The metal ion speciation increases due to greater availability of the active sites at higher concentration of adsorbent³¹.

3.5 Effect of initial metal concentration on Adsorption:

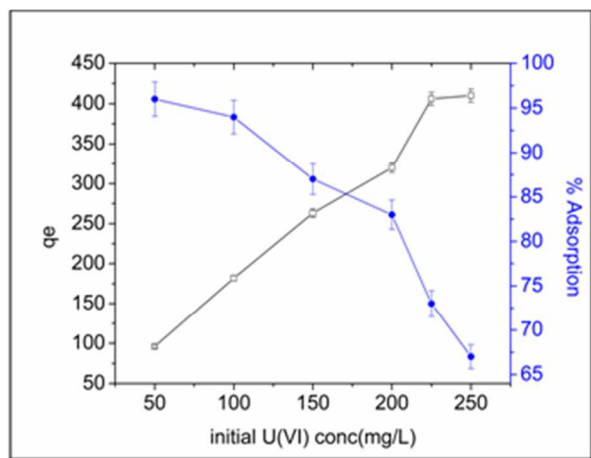


Fig. 9- Effect of initial U(VI) concentration on adsorption

The adsorption behavior of U(VI) ion on cellulose nanofibers was observed in concentrations ranging from 50mg/l to 250mg/l at a fixed initial pH of 6. The adsorption efficiency of the sorbent was observed to diminish whereas the adsorption capacity enhanced with increase in the initial U(VI) ion concentration (Fig.9). As a rule, increasing the initial metal ion concentration results in an increase in the adsorption capacity since it provides a driving force to overcome all mass transfer resistances of metal ions between the aqueous and solid phase³³. However, the sorption efficiency decreases since the adsorbent has a limited number of active sites, which saturates at a higher i.e. 225mg/L U(VI) concentration. The maximum adsorption was observed at 50mg/l and was noted to be 96%. Maximum adsorption capacity was found to be 410 mg/g under optimized experimental conditions (pH-7, sorbent dosage- 50mg, camphor content- 0.1wt%) of 250 mg/l U(VI) ion concentration using 100 ml of solution at an equilibrium time of 60 min.

3.6 Adsorption Isotherms

Adsorption mechanism can be described by adsorption isotherms data for the interaction of metal ions on the adsorbent surface and to determine the efficiency of adsorption. Collection of these data at different U(VI) concentrations were modeled using Langmuir, Freundlich, Temkin and Dubinin-Radushkevich adsorption models³²⁻³³.

$$\text{Langmuir: } q_e = \frac{q_{\max} K_L C_e}{1 + K_L C_e} \quad (3)$$

$$\text{Freundlich: } q_e = (K_F C_e)^{1/n} \quad (4)$$

$$\text{Temkin: } q_e = \frac{RT}{b_T} \times \ln(a_T C_e) + \frac{RT}{b_T} \ln C_e \quad (5)$$

$$\text{Dubinin- Radushkevich: } q_e = q_{\max} e^{(-K_D \varepsilon^2)} \quad (6)$$

Where, q_e is the amount of U(VI) adsorbed (mg/g); q_{\max} is equal to q_e for a complete monolayer (mg/g); K_L is a constant related to the affinity of the binding sites (L/mg); C_e is the equilibrium metal ion concentration (mg/L). K_F (related to adsorption capacity) and n (related to intensity) are Freundlich constants indicating adsorption capacity and intensity. R is the universal gas constant = $8.314 \times 10^{-3} \text{ kJ mol}^{-1} \text{ K}^{-1}$; T is absolute temperature (= 303K); b_T is the Temkin constant related to the heat of adsorption (kJ mol^{-1}); a_T is the equilibrium binding constant corresponding to the maximum binding energy (l/g)³⁴⁻³⁷.

Langmuir adsorption isotherm gives a strong indication for monolayer formation and adsorption of metal ions over a homogeneous surface without interaction between the adsorbed molecules³⁴ whereas Freundlich Isotherm model explains the ratio of the amount of solute adsorbed onto a heterogeneous surface of given mass of sorbent to the concentration of solute in solution is different at different concentrations³⁵. Temkin Isotherm model represents the heat of adsorption that decreases linearly with the coverage of adsorbate and adsorbent interactions³⁶. In D-R model, Dubinin³⁷ proposed the isotherm model to estimate the mean free energy of adsorption.

The linearized form of all the adsorption isotherm models can be defined as:

$$\text{Langmuir adsorption isotherm: } \frac{C_e}{q_e} = \frac{1}{q_{\max} K_L} + \frac{C_e}{q_{\max}} \quad (7)$$

Where, the Langmuir constants q_{\max} and K_L is obtained by linear regression method have been given in Table 1. Hall et al.³⁸ defines a constant R_L for expressing the essential features of Langmuir isotherm. R_L is a dimensionless constant separation factor or an equilibrium parameter calculated as:

$$R_L = \frac{1}{1 + K_L C_0} \quad (8)$$

From Table 1 and Fig. 10, The regression coefficient value (R^2) is calculated as 0.9946 for U(VI) ion. The R_L value obtained for U(VI) is 0.5166 which means that the model is in very close approximation with the adsorption experiment and falls in the favorable adsorption category.

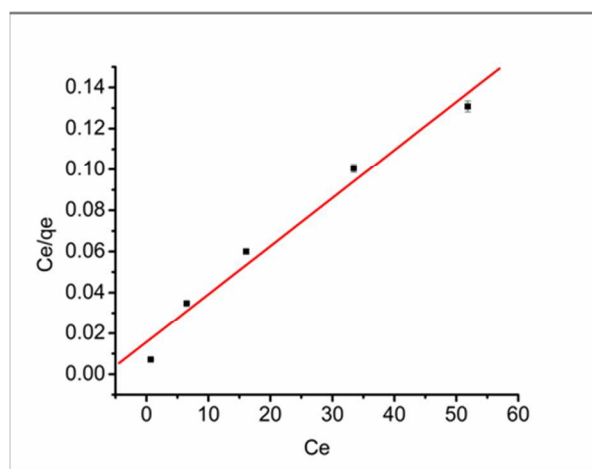


Fig. 10: Langmuir adsorption isotherm

$$\text{Freundlich isotherm model: } \ln q_e = 1/n \ln C_e + \ln K_F \quad (9)$$

Where, the linear plot (Fig. 11) of $\ln q_e$ vs. $\ln C_e$ gives the slope and intercepts values corresponding to $1/n$ and $\ln K_F$ respectively.

When $1/n = 1$, the value of K_F depends on the units in which C_e and q_e are expressed. Favorable adsorption represents that 'n' value in between 1 and 10. Larger n value (implying smaller $1/n$ value) means strong interaction between sorbent and metal ions while $1/n = 1$ represents linear adsorption i.e. identical adsorption energies at all sites³⁹. From Table 1, the regression coefficient value (R^2) obtained as 0.9982 for U(VI) ion i.e. adsorption experiment is significantly fit for Freundlich Isotherm model and positive value of n (2.02) meaning strong interaction between the fibers and U(VI) ion.

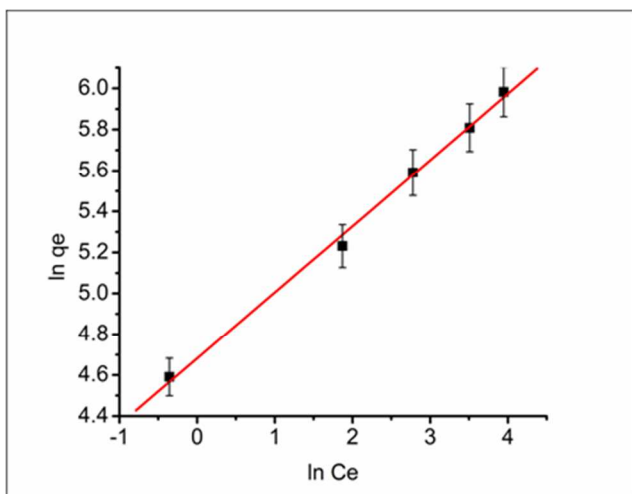


Fig. 11: Freundlich adsorption isotherm

A Linear plot (Fig. 12) of q_e vs. $\ln C_e$ in Temkin model assumes that the adsorption process is uniformly distributed and the fall in heat of adsorption is linear and not logarithmic as shown in the Freundlich model. Typical bonding energy range for ion exchange mechanism/ chemisorption is reported to be in the range of 8-16 kJmol^{-1} while physisorption processes are reported to have adsorption energies less than -40 kJmol^{-140} . This model enables to determine the constant A_T , B_T and b_T values presented in Table 1 suggested that adsorption involves chemisorption and physisorption of metal ions³².

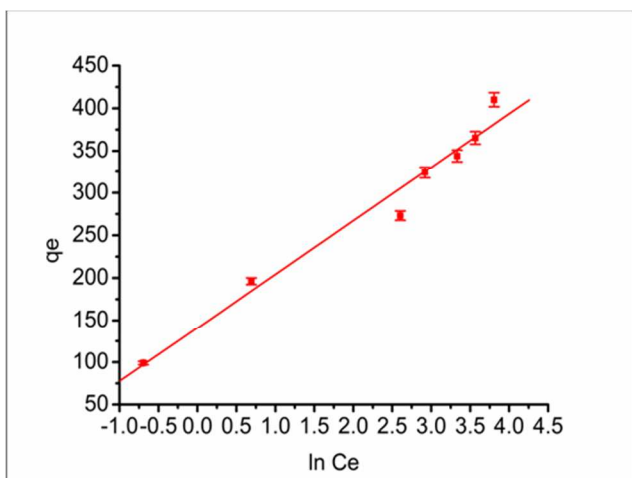


Fig. 12: Temkin adsorption isotherm

$$\text{D-R model: } \ln q_e = \ln q_{\max} - K\varepsilon^2 \quad (10)$$

Where, $K (\text{mol}^2\text{kJ}^{-2})$ is a constant related to the mean adsorption energy and ε is the Polanyi potential, which can be calculated from equation –

$$\varepsilon = RT \ln\left(1 + \frac{1}{C_e}\right) \quad (11)$$

The plot (Fig. 13) between $\ln q_e$ and ε^2 at 303 K temperature gives the values of K and q_{\max} . K is a constant which yields the mean free energy of sorption, E , per molecule of the adsorbate when it is transferred to the surface of the solid from infinity in the solution. It can be calculated as follows:

$$E = 1/\sqrt{2K} \quad (12)$$

From the plot, the value of K are calculated as 55.31×10^{-6} and $E=9.4696 \text{ kJ/mol}$ reflects the chemisorption nature of the process, similarly, R^2 value are obtained as 0.9932 suggesting that the isotherms could be more appropriate under industrial conditions. The adsorption of U(VI) ion over cellulose – camphor soot nano fibers is a good fit for D-R model⁴¹.

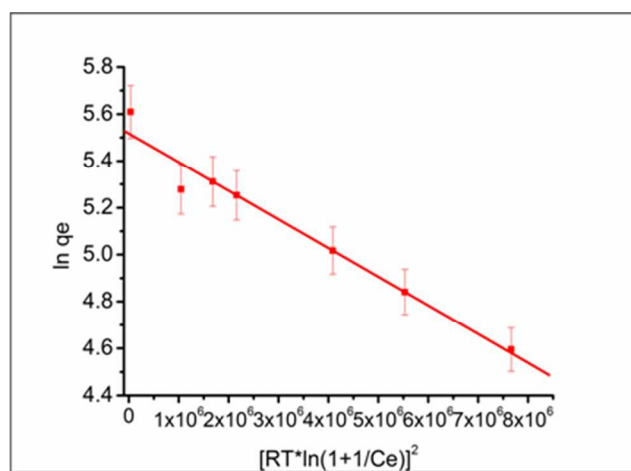


Fig. 13: Dubinin- Rudushkevich adsorption isotherm

The above result indicates that the adsorption of U(VI) ion over cellulose – camphor soot fibers is in good agreement with all above discussed Isotherm models. The Freundlich Isotherm model Regression coefficient is greatest in magnitude equal to 0.9982 suggesting that there is heterogeneous adsorption of U(VI) ion via a physiochemical adsorption process but more reflecting towards chemisorption nature of the process involving the oxides and acetate groups of the fibers. The Equilibrium Isotherm curves and parameters for various models have been represented in Fig. 10, 11, 12, 13 and Table 1 respectively.

Table 1: Equilibrium Adsorption constants

Adsorption Isotherm	Isotherm parameters	U(VI)
Langmuir	q_{\max} (mg/g)	5.1616
	K_L (L/mg)	0.0616
	R_L	0.5166
	R^2	0.9946
Freundlich	n	2.02
	K_F (mg/g)	0.8634
	R^2	0.9982
Temkin	B_T (J/mol)	1.593
	a_T (L/min)	0.889
	R^2	0.9987
Dubinin-Radushkevich	q_{\max} (mg/g)	166.21
	$K \times 10^{-6}$ (mol ² kJ ⁻²)	55.31
	R^2	0.9932
	E (kJ/mol)	9.4696

* R_L , R^2 , n are dimensionless

3.7 Kinetic Studies:

The Kinetic parameters are essential for the prediction of adsorption rate and give important information for designing and modeling the batch process⁴². Several kinetic models (Pseudo – first order kinetics, Pseudo – second order kinetics, Elovich and Intraparticle diffusion model) have been applied to determine the rate controlling mechanism of the adsorption process.

3.7.1. Pseudo first order kinetic model:

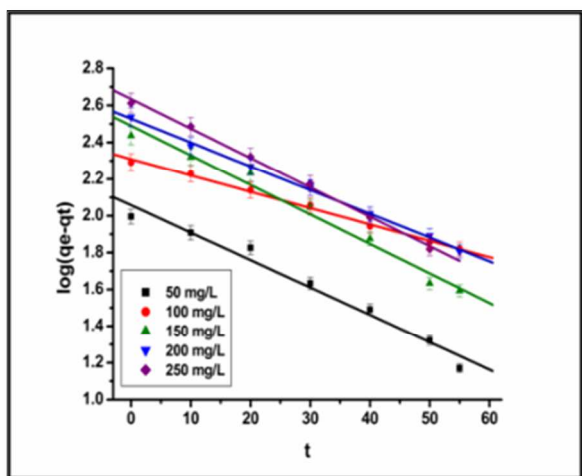


Fig. 14: Pseudo first order kinetic model

Pseudo first order model of Lagergren showed that the rate of adsorption of solute on the adsorbent is based on the adsorption capacity. Also, this model is used to estimate the k_{ad} value which

is the mass transfer coefficient in the design calculations⁴³. The rate equation of pseudo first order is expressed as:

$$\log(q_e - q_t) = \log q_e - \left(\frac{k_1}{2.303}\right)t \quad (13)$$

Where, q_e = adsorption capacity at equilibrium time (mg/g); q_t = adsorption capacity at time t (mg/g) and k_1 is the first-order adsorption rate constant (min^{-1}).

A plot of (Fig. 14) $\log(q_e - q_t)$ vs. t gives a linearized form. From the slope, Pseudo – first – order rate constant and the intercept gives the value of q_e . The obtained values of q_e and k_1 are mentioned in Table 2. The experimental and the theoretical q_e values are in concordance with one another suggesting that the adsorbent process follow pseudo – first order kinetics⁴¹.

3.7.2 Pseudo second-order kinetic model:

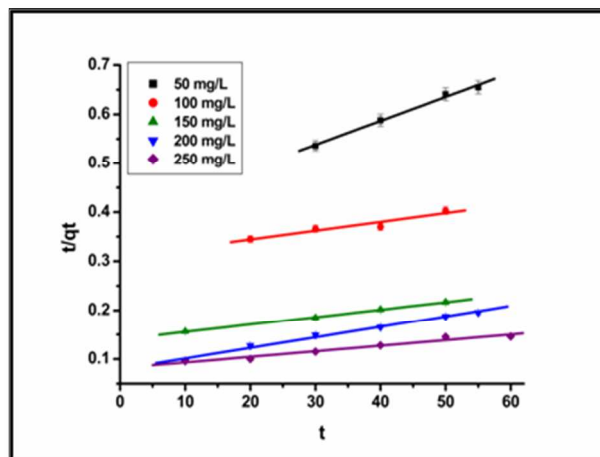


Fig. 15: Pseudo second order kinetic model

Pseudo second-order reaction given by Ho and McKay is highly influenced by the amount of adsorbate on the surface of the adsorbent and the amount of adsorbate adsorbed at equilibrium. The rate is directly proportional to the number of active sites on the surface of the adsorbent⁴⁴. The pseudo second-order equation is given as:

$$\frac{t}{q_t} = \frac{1}{k_2 q_e} + \frac{t}{q_e} \quad (14)$$

Where, k_2 is the second-order adsorption rate constant ($\text{g mg}^{-1} \text{min}^{-1}$). The constant k_2 can calculate the initial sorption rate ' h ' ($\text{mg}/(\text{g min})$) at $t \rightarrow 0$ in the following equation –

$$h = k_2 q_e \quad (15)$$

The linear regression values (R^2) are less than 0.9 suggesting that the adsorption process deviates from the Pseudo – Second order kinetic model. The experimental and theoretical q_e values (Fig. 15) do not match further suggesting that the adsorption process does not follow pseudo – second order kinetics.

3.7.3 Elovich model:

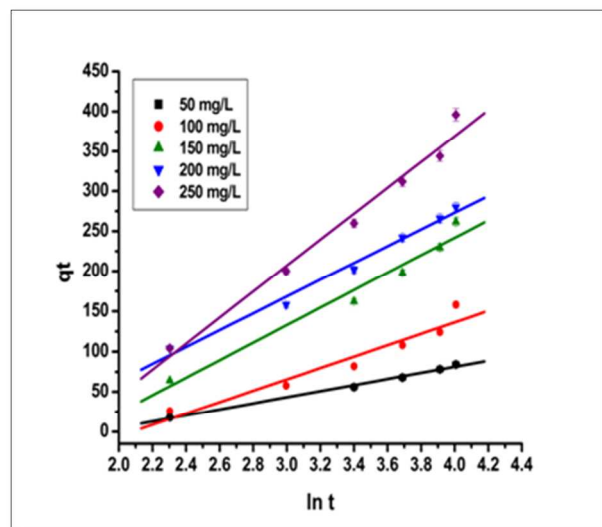


Fig. 16: Elovich kinetic model

The Elovich model is one of the most useful models in describing such 'activated' chemisorption. Elovich equation⁴⁵ is a rate equation based on the adsorption capacity describing the adsorption on highly heterogeneous adsorbent –

$$\frac{dq_t}{dt} = \alpha e^{-\beta q_t} \quad (16)$$

Where, α ($\text{mg g}^{-1} \text{min}^{-1}$) is the initial adsorption rate and β (g/mg) is the desorption constant related to the extent of surface coverage and activation energy for chemisorption.

The linearized form of the above equation is given as

$$q_t = \frac{\ln \alpha \beta}{\beta} + \frac{\ln t}{\beta} \quad (17)$$

Assuming $\alpha \beta \gg t$ and $q_t=0$ at $t=0$, Eq. (17) gives a linearized graph (Fig. 16) of q_t vs. $\ln t$ from the slope and intercept. As mentioned in table 2, the regression coefficients at all concentrations show close proximity of the adsorbance reactions to the Elovich kinetic model³².

3.7.4 Intraparticle mass transfer diffusion model:

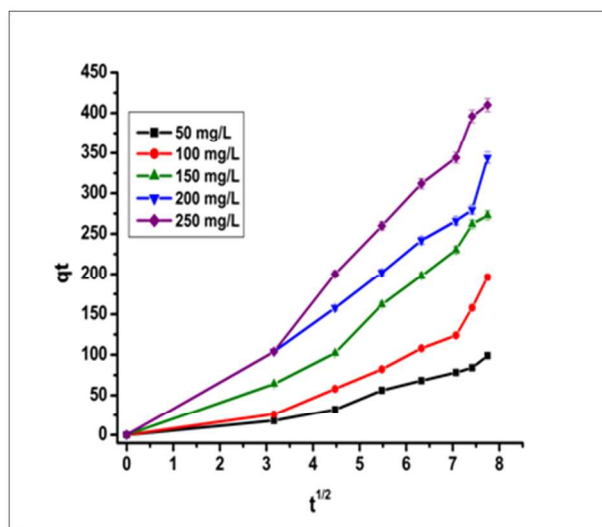


Fig. 17: Intraparticle diffusion model

Intraparticle mass transfer diffusion model are used for identifying the adsorption mechanism of U(VI) ions onto cellulose-carbon soot adsorbent. According to Weber and Morris⁴⁶, Intraparticle diffusion coefficient k_{id} is given by the following expression:

$$q_t = K_{int} t^{1/2} \quad (18)$$

Where, K_{int} is the intra-particle diffusion rate constant ($\text{mg g}^{-1} \text{min}^{-0.5}$). The plots (Fig. 17) of q_t versus $t^{1/2}$ at various initial concentrations of U(VI) ion presents multi-linearity in the graph indicating occurrence of two or more steps in the adsorption process⁴⁷. The sharper portion represents external surface adsorption or instantaneous adsorption. The gradual adsorption stage describes the rate controlling step of Intraparticle diffusion. Third sharper portion gives the final equilibrium stage where intraparticle diffusion process begins to slow down due to extremely low concentration of adsorbate in the solution. As shown in Fig.17, no gradual or third sharper portion was seen which means only instantaneous adsorption takes place whereas, rate controlling step and equilibrium stage are absent.

Table 2: Kinetic parameters for adsorption of U(VI) ion

	Conc.	50	100	150	200	250
Pseudo first-order	$q_e(\text{mg/g})$	343.6	342.6	409.8	456.9	482.2
	$K_1(\text{min}^{-1})$	0.069	0.021	0.045	0.036	0.048
	R^2	0.996	0.998	0.996	0.098	0.962
Pseudo second-order	$q_e(\text{mg/g})$	288.6	678.9	692.2	594.98	893.0
	$K_2(\text{g/mg min})$	0.021	0.011	0.023	0.0381	0.038
	R^2	0.886	0.843	0.892	0.8764	0.890
Elovich	Σ	0.160	0.213	0.268	0.387	0.675
	θ_c	0.039	0.04	0.089	0.134	0.239
	R^2	0.997	0.996	0.973	0.9350	0.990
Intraparticle diffusion	$K_{int}(\text{mg g}^{-1} \text{min}^{-0.5})$	22.12	38.52	56.78	53.45	68.03
	R^2	0.930	0.883	0.930	0.9654	0.967

3.8 Adsorption Thermodynamics

Thermodynamic parameters such as enthalpy and entropy which reflect the spontaneity of a reaction were determined based on Van't Hoff plot using the following equations⁴⁸⁻⁵⁰.

$$\Delta G^0 = -RT \ln K_L \quad (19)$$

$$\ln K_L = \Delta S^0/R - \Delta H^0/RT \quad (20)$$

Where, K_L is the equilibrium constant obtained from Langmuir isotherm; R = Universal gas constant = $8.314 \text{ Jmol}^{-1} \text{K}^{-1}$; T = Absolute temperature = 303 K ; ΔG^0 is Gibb's free energy change (J/mol); ΔS^0 (J/mol K) and the ΔH^0 (J/mol) are the standard entropy and enthalpy of the adsorption. The free energy values were obtained for uptake of U(VI) ion is -6.618 KJ/mol which shows the feasibility and spontaneity of the reaction. Positive value of ΔH^0 (22.43 kJ/mol) confirms endothermic process and shows a strong interaction between U(VI) ions and cellulose-camphor soot fibers. The positive value of ΔS^0 (97.3 J/mol/K) reveals increased state of randomness or disorderness at the solid-solution interface during adsorption of U(VI) onto cellulosic nanofibers. Thereafter, it was found that $\Delta H^0 < T\Delta S^0$, attributes

entropy is more considerable than enthalpy of activation in the adsorption process. The present study predicts the spontaneous, feasible and endothermic nature of the sorption processes based on numerical value of ΔG^0 , ΔH^0 and ΔS^0 .

3.9 Desorption Experiments:

For the reusability of nano fibrous membrane and recovery of U(VI) ions, desorption experiments were conducted with a series of varied reagents as shown in Table 3. Among the various reagents used, 0.1M CH_3COOH and 0.1M HCOOH effectively recover the U(VI) ions at pH 6.0 adsorbed by Cellulose- nano fibers. 95.8% and 98.4% of U(VI) ions were recovered by using 0.1M CH_3COOH and HCOOH due to displacement of H^+ by U(VI) ion and formation of stable Uranium acetate and Uranium formate complexes. The results (shown in Fig.18) revealed that desorption percentage increases from 59% to 98% within 30 min, thereafter, equilibrium is achieved i.e. no change in desorption yield (Fig.18). Therefore, U(VI) ions could be desorbed successfully by using 0.1M CH_3COOH and HCOOH and effectively used for the regeneration of the nano fibers.

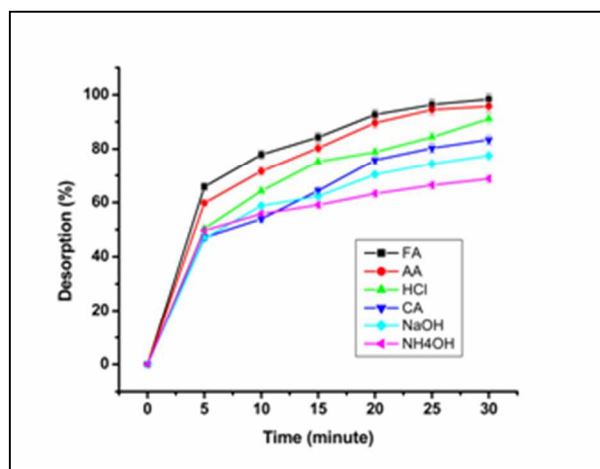


Fig. 18- Effect of contact time on % desorption of U(VI) ions

Table 3: Percentage of adsorbed U(VI) ions desorbed from cellulose- camphor soot fibers by different reagents

Reagent	Contact time (min)	Desorption (%)
HCOOH	5	65.8
	15	84.3
	30	98.4
CH_3COOH	5	59.8
	15	80.32
	30	95.81
HCl	5	50.3
	15	75.2
	30	85.73
Citric Acid	5	47.1
	15	64.4
	30	83.45
NaOH	5	46.7
	15	62.32
	30	77.5
NH_4OH	5	49.6
	15	59.1
	30	68.8

4. Conclusions

In this study the novel adsorbent electrospun nonwoven nanofibers was synthesized and characterized through FESEM, FT-IR, XRD and Raman spectroscopy. The effectiveness of nonwoven fibers was tested for reclamation and recovery of U(VI) ions from aqueous streams. Batch experiments were conducted with an adsorbent dosage of 50mg/l. Maximum adsorption for U(VI) ion was found at pH 6. The Quantitative adsorption capacity was found to be 410mg/g with 96% adsorption at varying concentration within a period of 60min. The adsorption kinetics indicated good agreement with Pseudo first order and Elovich model. Pseudo second order model showed very little or no agreement with regression coefficient and q_{max} values. Similarly, Mass transfer diffusion model showed that there is an excellent monolayer dispersion of U(VI) ions on the adsorbent which clearly indicates that there was no equilibrium attained even after 120 minutes, which meant that adsorption process was still in the instantaneous adsorption phase. Equilibrium isotherm data were analyzed by Langmuir, Freundlich, Temkin and Dubinin Rudushkevich which showed that the Adsorption process was in good agreement with all models although the q_{max} value in the D-R model showed large deviation from the experimental q_{max} value. With a regression coefficient of 0.9982, the Adsorption process was in maximum agreement with the Freundlich isotherm via physicochemical process. Thermodynamics parameters indicated a highly spontaneous and feasible adsorption reaction. The reusability of cellulose fibers was examined for economic viability and practical potential by treating with 0.1M CH_3COOH and 0.1M HCOOH . It was concluded that cellulose-camphor soot fibers is an effective adsorbent for the reclamation and recovery of U(VI) ions from aqueous streams.

Acknowledgements

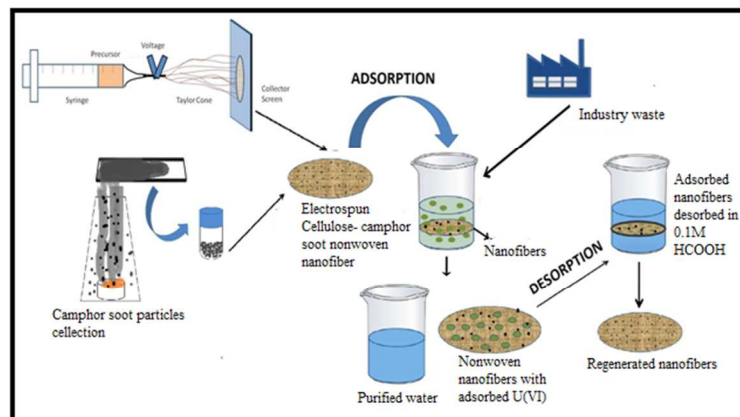
The authors appreciate Defence Institute of Advanced Technology for financial support. Also would like to thanks Dr. Prahlada, Vice Chancellor, DIAT-DU for continuous encouragement and support. We are also grateful to Dr. R.R. Gonte, Dr. P. Alegaonkar, Dr. A. Abhyankar, D D Gunjal Suwarna Raut and Professor Dhola (University of Pune) for continuous technical support.

Notes and references

- [1] N. Raje and A. V. R. Reddy, *Thermochim. Acta* 2010, 505, 53.
- [2] T. P. Rao, P. Metilda, and J. M. Gladis, *Talanta* 2006, 68, 1047.
- [3] Metaxas, M.; Rigopoulos, V. K.; Galiatsatou, P.; Konstantopoulou, C.; Oikonomou, D. J. *Hazard. Mater.* 2006, B97, 71.
- [4] Anirudhan, T. S.; Rajeena, S. R., *Ind. Eng. Chem. Res.* 2011, 50, 13288
- [5] A. Ayalew, R. R. Gonte, and K. Balasubramanian, *J. Polymers* 2012, 4, 440.
- [6] S. Onal, S. H. Baysal, and G. Ozdemir, *J. Hazard. Mater.* 2007, 146, 417.
- [7] S. Xie, J. Yang, C. Chen, X. Zhang, Q. Wang, and C. Zhang, *J. Environ. Radioact.* 2008, 99, 126.
- [8] M. H. Khani, A. R. Keshtkar, M. Ghannadi, and H. Pahlavanzadeh, *J. Hazard. Mater.* 2008, 150, 612.
- [9] K. Akhtar, M. Waheed Akhtar, and A. M. Khalid, *Water Res.* 2007, 41, 1366.
- [10] C. İslek, A. Sinağ, and I. Akata, *CLEAN – Soil, Air, Water* 2008, 36, 387.

- [11] Y.-H. Wang, S.H. Lin, and R.-S. Juang, *J. Hazard. Mater.* 2003, 102, 291.
- [12] B. N. Sahoo, *Express Polym. Lett.* 2013, 7, 900.
- [13] Terrones, A; 2003 *Annu. Rev. Mater. Res* 2003, 33, 419.
- [14] Li, W.Z.; Xie, S.; Quin, L. X.; Chang, B. H.; Zou, B. S.; Zhou, W. Y. *Science* 1996, 274,1701.
- [15] Kong, J.; Cassall, A. M.; Dai, H. *Chem. Phys. Lett.*1998, 292,567.
- [16] J.R. Lloyd, L.E.Mackaskie, D.R. Loveley (Ed.), *Environmental Metal microbe Interaction*, Am. Soc. of Microbiology, Washington, DC, 2000, pp. 277-327.
- [17] B.N.Sahoo, K. Balasubramanian, *RSC Advances* 2014, 4, 11331.
- [18] Yadav, R., Balasubramanian, K. *Mater. Lett.* 2013, 110, 130.
- [20] Sahoo, B.N.; Kandasubramanian, B.; Sabarish, B. *Expr. Poly. Lett.* 2013, 7, 900.
- [21] Sen, R.; Govindraj, A.; Rao, C. N. R. *Chem. Phys. Lett.* 1997, 267, 276.
- [22] Gonte RR, Balasubramanian K, Mumbreakar JD. *Journal of Polymers* 2013, DOI: 10.1155/2013/309136.
- [23] Shooto D. N.; Dikio E. *D.Int. J. Electrochem. Sci.*, 2011, 6, 1269.
- [24] Manoj, B.; S.; Anu. N.M.; Kunjomana, A.G. *Int. J. Electrochem. Sci.* 2012, 7, 3215.
- [25] Fourest, E.; Volesky, B. *Environ. Sci Technol.*1996, 30, 277.
- [26] Arnold, P.L.; Love, J, B.; Patel, D. *Coord. Chem. Rev.* 2009, 253, 1973.
- [27] Chen, P.; Huang, F.; Yun, S. *Carbon* 2003, 41, 2093.
- [28] Langmuir I. *Journal of Am. Chem. Soc.* 1916, 38, 2221.
- [29] Wong, K. K., Lee, C. K., Low, K. S. and Haron, M. J. *Chemosphere* 2003, 50, 23.
- [30] A. Saeed, Muhammed Iqbal, and M. Waheed Akhtar, *Hazardous Materials* 2004, 117, 65.
- [31] Abdel-Ghani, N. T., M. Hefray, G. A. F. *EL-Chaghaby Int. J. Environ. Sci. Tech.* 2007, 4, 67.
- [32] T.S. Anirudhan, P.S. Suchitra, P.Senan and A.R.Tharun., *Ind. Eng. Chem. Res.*, 2012, 51, 4825.
- [33] Gonte RR, Shelar G, Balasubramanian K., *Desalination and Water Treatment* 2013, DOI: 10.1080/19443994.2013.833876.
- [34] Kumar, M.; Ando, Y. *Carbon* 2005, 43, 533.
- [35] Boparai, H.K., Joseph, M., O'Carroll, D.M., *J. Hazard. Mater.* 2011, 186, 458.
- [36] Liu, Y.; Liu, Y. J., *Sep. Purif. Technol.* 2008, 61, 229.
- [37] Kaygun, A. K.; Akyil., S. *J. Hazard. Mater.* 2007, 147, 357.
- [38] K.R. Hall, L.C. Eagleton, A. Acrivos, T.Vermeulen, *Ind. Eng. Chem. Fundam.*1996, 5, 212.
- [39] Balasubramanian. K.; Gonte RR.; Bhalara. P.; Punetha. D., *Indian Patent*, 2735/MUM/2013.
- [40] B. Kiran, A. Kaushik, *Biochem. Eng. J.* 2008, 38, 47.
- [41] A. Benhamou, M. Baudu, Z. Derriche, J.P. Basly, *J. Hazard. Mater.* 2009, 171, 1001.
- [42] G.D. Hasley, *Adv. Catal.* 1952, 4, 259.
- [43] B.P. Bering, M.M. Dubinin, V.V.Serpinsky, *J.colloid Interface. Sci.* 1972, 38, 185.
- [44] Ho, Y.S., McKay, G., *Process Biochem.* 1999, 34, 451.
- [45] S. Rengaraj, J. W. Yeon, Y. Kim, Y. Jung, Y.K. Ha, W. H. Kim, *J. Hazard. Mater.* 2007, 143, 469.
- [46] O. Hamdaoui, M. Chiha, *Acta Chim. Slov.* 2007, 54, 407.
- [47] Bhatnagar, A.; Jain, A. K., *J. Colloid Interface Sci.* 2005, 281, 49.
- [48] W.J. Weber, J.C. Morris, *J. Sanit. Eng. Div. Am. Soc. Civ. Eng.* 1963, 89, 31.
- [49] Khan, S. A.; Ur- Rehman, R.; Khan, M. A., *Waste Manage.* 1995,15, 271.
- [50] Cao Q.; Liu Y.; Wang C.; Cheng J.; *J. Hazard. Mater.* 2013, 263, 311.

75 Graphical abstract:



5

10

15 Figure caption

Fig. 1- (a) Open structure of camphor soot (b) Ring structure of camphor soot

Fig. 2- FESEM Images (a) cellulose electrospun fibers (b) cellulose loaded with camphor soot fibers (c and d) magnified view of CCSF

Fig. 3- IR Spectra of cellulose fibers, camphor soot particles, cellulose-camphor soot fibers (CCSF) and U(VI)- CCSF.

Fig. 4- XRD Patterns of cellulose, camphor- soot particles, cellulose-camphor soot fibers

Fig. 5- Raman spectra of (a) camphor soot particles and (b) cellulose acetate fibers

Fig. 6- Effect of pH on adsorption (a) cellulose acetate fibers (b) pH of CCSF

Fig. 7- Camphor soot loading

Fig. 8- Adsorbent dosage

Fig. 9- Effect of initial U(VI) concentration on adsorption

Fig. 10- Langmuir adsorption isotherm

Fig. 11- Freundlich adsorption isotherm

Fig. 12- Temkin adsorption isotherm

Fig. 13- Dubinin- Rudushkevich adsorption isotherm

Fig. 14- Pseudo first order kinetic model

Fig. 15- Pseudo second order kinetic model

Fig. 16- Elovich kinetic model

Fig. 17- Intraparticle diffusion model

Fig. 18- Effect of contact time on % desorption of U(VI)

45